Journal of Anatomy

J. Anat. (2019) **235**, pp670–685 doi: 10.1111/joa.13011

Callosal septa express guidance cues and are paramedian guideposts for human corpus callosum development

Marko Culjat[1] and Nataša Jovanov Milošević[2]

[1]*MedStar Georgetown University Hospital, Washington, DC, USA*
[2]*Croatian Institute for Brain Research, School of Medicine, University of Zagreb, Zagreb, Croatia*

Abstract

The early development and growth of the corpus callosum are supported by several midline transient structures in mammals that include callosal septa (CS), which are present only in the second half of gestation in humans. Here we provide new data that support the guidance role of CS in corpus callosum development, derived from the analysis of 46 postmortem fetal brains, ranging in age from 16 to 40 post conception weeks (PCW). Using immunohistochemical methods, we show the expression pattern of guidance cues ephrinA4 and neogenin, extracellular protein fibronectin, as well as non-activated microglia in the CS. We found that the dynamic changes in expression of guidance cues, cellular and extracellular matrix constituents in the CS correlate well with the growth course of the corpus callosum at midsagittal level. The CS reach and maintain their developmental maximum between 20 and 26 PCW and can be visualized as hypointense structures in the ventral callosal portion with *ex vivo* (*in vitro*) T2-weighted 3T magnetic resonance imaging (MRI). The maximum of septal development overlaps with an increase in the callosal midsagittal area, whereas the slow, gradual resolution of CS coincides with a plateau of midsagittal callosal growth. The recognition of CS existence in human fetal brain and the ability to visualize them by *ex vivo* MRI attributes a potential diagnostic value to these transient structures, as advancement in imaging technologies will likely also enable *in vivo* MRI visualization of the CS in the near future.

Key words: axon guidance; fetal human brain; fetal magnetic resonance imaging; midline glia; subcallosal zone.

Introduction

Corpus callosum (CC) is a commissural fibre tract specific to eutherian mammals. An increase in its size mirrors the expansion of the isocortical areas and their connectivity throughout mammalian evolution, and reaches its maximum complexity, fibre number, and size, relative to brain volume, in humans (for review see Gazzaniga, 2000; Suarez et al. 2014). The CC is the largest commissural tract in the human brain, containing approximately 200–300 million axons in the adult (Aboitiz et al. 1992; Aboitiz & Montiel, 2003). Animal studies have shown that callosal axons originate from a diverse population of neocortical pyramidal neurons whose cell bodies reside in cortical layers II/III (approximately 80% in rodents), layer V (approximately 20% in rodents) and, to a lesser extent, layer VI (Lamantia & Rakic, 1990; LaMantia & Rakic, 1990; Koester & O'Leary, 1994; Rash & Richards, 2001; Richards et al. 2004; Lindwall et al. 2007; Donahoo & Richards, 2009; Fame et al. 2011; Leyva-Diaz & Lopez-Bendito, 2013). Anatomical studies in primates, including humans, have shown that the majority of callosal axons originate from pyramidal neurons, mostly from layer III pyramidal neurons that connect contralateral homotypic areas, and, to a lesser extent, heterotypic cortices, and finally, a small proportion of callosal axons arise form migrating neurons during development (Hedreen & Yin, 1981; Schwartz & Goldman-Rakic, 1991; Schwartz et al. 1991; Schmahmann & Pandya, 2006; Wahl et al. 2007). Diffusion tensor tractography imaging (DTI) studies have shown that the callosal axons are topographically organized along the anteroposterior axis and homotopically link contralateral cortical regions in the Rhesus monkey (Hofer et al. 2008) and in healthy humans (Hofer & Frahm, 2006; Huang et al. 2009), and heterotopically, in patients with partial callosal agenesis (Wahl et al. 2009). Combining anatomical and MRI DTI methods, three types of callosal

Correspondence
Nataša Jovanov Milošević, Croatian Institute for Brain Research, School of Medicine, University of Zagreb, Salata12, Zagreb, Croatia.
T: + 385 914596 816; E: njovanov@hiim.hr

Accepted for publication *9 April 2019*
Article published online *9 May 2019*

fibres in the frontal portion of the CC have been described: (1) homotopic dorso-medial fibres that connect the medial areas; (2) ventro-lateral homotopic and heterotopic fibres, distributed to the ventral regions of the frontal lobes and (3) ventro-striatal heterotopic fibres that connect the dorsal frontal lobe with the contralateral head of the caudate nucleus and putamen (De Benedictis et al. 2016).

The corpus callosum is composed of axons of various calibres, but most have a similar diameter below 1 μm, as confirmed by different measurement techniques (Aboitiz et al. 1992; Caminiti et al. 2009; Liewald et al. 2014). In monkeys, chimpanzees and humans, callosal axons of distinct sizes interconnect functionally different cortical areas. Thinner axons in the genu and in the posterior body of the CC interconnect the prefrontal and parietal areas, respectively, and thicker axons in the midbody and in the splenium interconnect primary motor, somatosensory and visual areas (Caminiti et al. 2009).

The initial formation of the CC in human is preceded by midline fusion above the septal area, which results in the formation of the massa commissuralis (Rakic & Yakovlev, 1968), followed by the differentiation of several medially positioned transient structures, described in rodent models, and their equivalents in humans: midline zipper glia, glial wedge, glial-neuronal sling and indusium griseum glia (Silver et al. 1982; for review see Shu et al. 2003; Suarez et al. 2014). These structures enable and support the first *pioneer* callosal axons, which originate in the cingulum (Koester & O'Leary, 1994; deAzevedo et al. 1997; Rash & Richards, 2001; Piper et al. 2009), to cross the midline and later serve as guides for the *follower* callosal axons.

The location at which early callosal axons cross the midline is determined by differential concentrations of diffusible morphogens, primarily Wnt/BMP, Shh and FGF (for review see Suarez et al. 2014), whereas the further development of the CC is critically regulated by the differential expression of guidance cues in the guidepost structures on the growth pathways, and by specific receptors on the growing callosal axons. The list of identified guidance ligands and receptors involved in corpus callosum formation in rodents and in humans is continuously expanding (see review articles by Judas et al. 2003; Plachez & Richards, 2005; Richards et al. 2004; Lindwall et al. 2007). For example, neogenin protein interacts with the repulsive guidance molecule (RGM) and with netrin-1 to guide axons within the embryonic vertebrate forebrain (Wilson & Key, 2006). Neogenin was found on several major axon tracts, such as the anterior commissure in the mouse brain (Van den Heuvel et al. 2013). The ephrin ligands/Eph receptors tyrosine kinases (EphRTK) family of guidance cues regulates neuron migration and guides axons along intermediate choice points, preventing cells and axons from entering inappropriate territories (for reviews see Klein & Kania, 2014; Kania & Klein, 2016). However, evidence for the expression of these molecules in the human brain midline is still lacking.

The topography of callosal axons along the dorso-ventral gradient is established early in development in both animal models (Richards et al. 2004) and humans (Tovar-Moll et al. 2007). In a normally developing mouse brain and humans, this topography is largely secondary to the medio-lateral location of the neuronal cell bodies from which callosal axons originate, in such a way that axons from medially located neurons cross the midline through the dorsal potions of the callosum, whereas laterally positioned neurons project through ventral portions of the CC (Zhou et al. 2013; De Benedictis et al. 2016). In the second half of gestation in humans, the growth of the CC proceeds in both the rostral/frontal and caudal/occipital directions, supported by additional zones: the subcallosal zone (SCZ), whose lateral aspects represent the dorsal allocortical equivalent of the subventricular zone (SVZ), most developed in humans (Kostovic et al. 2002) and, in human fetuses alone, a group of small, possibly primate-specific, structures called callosal septa (CS), which have been described within the ventral portion of the developing CC (Jovanov-Milosevic et al. 2006, 2009). Together, these two entities form grooves in which the growing callosal fascicles lie. Their strategic position, close proximity to growing CC axons, and cellular and extracellular composition suggest expression of multiple guidance molecules in the CS, and their involvement in the guidance of growing callosal axons in distinct intracallosal fascicles.

The clinical importance of the CC in humans is evidenced by changes in its macro- and microstructure, along with its functional characteristics seen in a wide range of conditions: e.g. preterm birth and related brain injury, genetic and metabolic conditions and non-syndromic developmental delay, agenesis of the corpus callosum (for review of genetic, developmental and functional aspects of callosal connectivity see Innocenti et al. 2003; Miller et al. 2005; Paul et al. 2007; Paul, 2011; Edwards et al. 2014).

In this article, our aim is to describe new findings related to the callosal septa, including their shape and the distribution of cellular elements, extracellular matrix and guidance molecules as well as their visualization by experimental *in vitro* 3T MRI, and to relate these findings to the course of corpus callosum growth in the midline.

Materials and methods

The 46 samples of postmortem fetal brains, ranging in age from 16 to 40 postconceptional weeks (PCW), used in this study are described in detail in Table 1. Fetal brain specimens were obtained following medically indicated or spontaneous abortion, or the demise of a prematurely born infant. None of the brains had any obvious macroscopic or microscopic anomalies. The sample collection was approved by the Institutional Ethical Review Board (EP02/21AG) of the School of Medicine and Clinical Hospital Center, University of Zagreb, in accordance with the Declaration of Helsinki 2000 and became part of the Zagreb Neuroembryological Collection (Judas et al. 2011). The developmental age expressed as PCW

Table 1 Record of analysed brain tissue.

Case No.	Use	Cause of death/comorbidities	Sex	Developmental age	ST	PMD
1	N	Spontaneous abortion	Female	16 PCW (18 WG)	/	12 h
2	N, Y	Tubal pregnancy	N/A	18 PCW (20 WG)	/	2 h
3	N, Y	Premature rupture of membranes	Female	18 PCW (20 WG)	/	6 h
4	N, Y	Chorioamnionitis	Female	20 PCW (22 WG)	/	24 h
5	N, Y	Premature delivery/heart failure	N/A	20 PCW (22 WG)	2 h	N/A
6	N	Premature delivery/respiratory insufficiency	Female	20 PCW (22 WG)	35 min	N/A
7	N	Chorioamnionitis	Female	20 PCW (22 WG)	/	9 h
8	N	Fetal demise	Male	21 PCW (23 WG)	/	9 h
9	N	Chorioamnionitis	Female	21 PCW (23 WG)	/	8 h
10	N, Y	Maternal clinical deterioration	Female	21 PCW (23 WG)	/	24 h
11	N	Fetal demise	N/A	21 PCW (23 WG)	/	10 h
12	N	Fetal demise	Male	21 PCW (23 WG)	/	N/A
13	N, Y	Premature separation of placenta	Male	22 PCW (24 WG)	/	9 h
14	N, Y	Fetal demise	Male	22 PCW (24 WG)	/	23 h
15	N	Fetal demise	Female	22 PCW (24 WG)	/	3 h
16	N, Y	Premature delivery	Female	22 PCW (24 WG)	27 min	N/A
17	N, Y	Fetal demise/heart failure	Female	23 PCW (25 WG)	/	N/A
18	N, Y	Premature separation of placenta	Female	23 PCW (25 WG)	/	6 h
19	N, Y	Chorioamnionitis	Male	24PCW (26 WG)	/	5 h
20	N, Y	Premature separation of placenta	Male	24 PCW (26 WG)	/	21 h
21	N, Y	Premature delivery/cardiorespiratory failure	Male	24 PCW (26 WG)	2 h	N/A
22	N, Y	Premature delivery/respiratory distress syndrome	Male	24 PCW (26 WG)	2 h	16 h
23	N, Y	Premature separation of placenta	Female	25 PCW (27 WG)	/	20 h
24	N, Y	Fetal demise	Female	25 PCW (27 WG)	/	14 h
25	N, Y	Premature delivery/cardiorespiratory insufficiency	Female	25PCW (27 WG)	10 h	8 h
26	N, Y	Premature delivery/cardiorespiratory insufficiency	Female	25 PCW (27 WG)	9 days	6 h
27	N, Y	Premature delivery/cardiorespiratory insufficiency	Male	26 PCW (28 WG)	8 h	N/A
28	N, Y	Fetal demise	Male	26 PCW (28 WG)	/	10 h
29	Y	Fetal demise	Male	26 PCW (28 WG)	/	N/A
30	Y	Asphyxia	Male	26PCW (28 WG)	/	N/A
31	Y	Fetal demise	Male	27 PCW (29 WG)	/	N/A
32	N, Y	Fetal demise	N/A	28 PCW (30 WG)	/	N/A
33	Y	Fetal demise	N/A	29 PCW (31 WG)	/	N/A
34	Y	Fetal demise	Male	30 PCW (33 WG)	/	24 h
35	N, Y	Premature delivery/cardiorespiratory insufficiency	N/A	30 PCW (32 WG)	3 h	19 h
36	N, Y	Fetal demise	Male	31 PCW (33 WG)	/	20 h
37	N, Y	Fetal demise	Male	33 PCW (35 WG)	/	24 h
38	N, Y	Premature separation of placenta	N/A	33 PCW (35 WG)	/	24 h
39	N, Y	Fetal demise	N/A	35 PCW (37 WG)	/	N/A
40	N, Y	Asphyxia	Male	37 PCW (39 WG)	9 days	N/A
41	N, Y	Fetal demise	Female	37 PCW (39 WG)	/	20 h
42	N, Y	Premature separation of placenta/stillborn	Male	40 PCW (42 WG)	/	7 h
43	N, Y	Premature separation of placenta/stillborn	Male	40 PCW (42 WG)	/	5 h
44	N, Y	Premature separation of placenta/cardiorespiratory insufficiency	Male	40 PCW (42 WG)	1 h	5 h
45	N, Y	Premature separation of placenta	Female	40 PCW (42 WG)	1 h	17 h
46	N, Y	Asphyxia	Male	40 PCW (42 WG)	/	2 h

N, case used for immunohistochemical staining with antibodies presented in Table 2; Y, case used to obtain midsagittal measures of corpus callosum (data shown in Fig. 5); PCW, postconception weeks; WG, weeks of gestation; ST, survival time; PMD, postmortem delay to fixation; N/A, data not available.

was estimated based on clinical pregnancy record and fetal crown–rump length. The commonly used gestational weeks (GW), equal to PCW plus 2 weeks, in Table 1 are given in brackets for the convenience of the clinical audience.

To obtain callosal midsagittal measures, fetal brains, extracted from the crania, were fixed for 48 h in 4% paraformaldehyde in 0.1 M phosphate-buffered saline (PBS; pH 7.4). Brains were then cut in the midsagittal plane and *in situ* CC were digitally photographed with a standard measure. Geometrical segmentation of the midsagittal callosal area and measuring of the segments is a verified method to study CC development and growth (Clarke et al. 1989; Witelson, 1989; Denenberg et al. 1991; Peters et al.

2000). We used the method described by Denenberg, which takes into account the curvature of the CC, and measured the thickness radial to the ventral surface of the corpus callosum. The digital photographs were processed with AutoCAD software to outline the CC borders, and to measure the size of the midsagittal surface area of the CC and the thicknesses of the genu, isthmus and splenium. We also measured the linear length of the callosum from the anterior-most point of the genu to the posterior-most point of the splenium. These measures of midsagittal CC at different time points were used to follow the overall callosal growth in order to compare it with the transient existence of septa and reveal their possible relationship.

For histological procedures, brains were cut into tissue blocks, embedded in paraffin, and cut in 20-μm-thick sections prior to staining. After the dewaxing of paraffin sections in alcohol, sections were rehydrated in PBS. The adjacent sections were processed and stained using either the Nissl method (cresyl violet) to delineate the histoarchitectural boundaries of the transient developmental compartments or immunohistochemical methods to demonstrate the CC axon growth, and immediate supporting structures: the CS and the subcallosal zone.

For immunohistochemistry, the rehydrated sections were first pretreated for 20 min in 0.3% hydrogen peroxide in a 3 : 1 mixture of methanol and redistilled water, then washed for 10 min in PBS, and immersed for 2 h in blocking solution (PBS containing 3% bovine serum albumin and 0.5% Triton X-100) at room temperature. The primary antibodies that were used in the study are described in detail in Table 2. The following primary antibodies were used to visualize growing callosal axons: mouse anti-microtubule-associated protein 2 (MAP2; 1 : 1000; clone HM2, Sigma-Aldrich, St. Louis, MO, USA); mouse anti-microtubule-associated protein 1B (MAP1B; 1 : 1000; clone AA6; Sigma-Aldrich); mouse anti-synaptophysin (1 : 100; clone SY38, Dako, Glostrup, Denmark); mouse anti-synaptosomal-associated protein 25 (SNAP25; 1 : 1000; clone SMI 81; Biolegend, San Diego, CA, USA); the polyclonal rabbit anti-growth associated protein 43 (GAP43, 1 : 1000; Novus Biologicals LLC, Centennial, CO, USA). To localize the relative regional distribution of glial cell populations, we used polyclonal rabbit anti-glial fibrillary acidic protein (GFAP; 1 : 1000; Dako) and mouse anti-human CD-68 (CD68; 1 : 80, Bio-Rad Antibodies Kidlington, Oxford, UK) for astroglia and microglia, respectively. To detect the presence of guidance cues in the CC and supporting callosal structures, two antibodies were used: polyclonal goat anti-neogenin (1 : 200, N-19, Santa Cruz Biotechnology, Inc., Dallas, TX, USA) and polyclonal rabbit anti-ephrinA4 (1 : 200, Santa Cruz Biotechnology). To detect extracellular content in the CS, polyclonal rabbit anti-human fibronectin primary antibody (1 : 400; Sigma-Aldrich) was used. Sections were incubated with primary antibodies for 18 h at 4 °C, washed in PBS, and further incubated with secondary antibodies for 1 h at room temperature. Finally, sections were incubated in Vectastain ABC reagent (streptavidin-peroxidase complex) for 1 h at room temperature and rinsed in PBS for 10 min. Biotinylated anti-rabbit and anti-mouse antibodies from the Vectastain ABC kit (Vector Laboratories Inc., Burlingame, CA, USA) were used to visualize specific immunoreactivity, as previously described (Jovanov-Milosevic et al. 2010; Kostovic et al. 2014). The peroxidase activity was visualized using Ni-3,3-diaminobenzidine (Sigma-Aldrich). Sections were dehydrated in a graded series of alcohols, cleared in xylene, and mounted with Histomount (National Diagnostics, Atlanta, GA, USA). Negative controls were included in all immunohistochemical experiments by replacing the primary antibody with the blocking solution or pre-immune goat or horse serum, by omitting the secondary antibody or by replacing it with an inappropriate secondary antibody; no immunoreactivity was detected in the control sections. Qualitative analysis of the stained histological sections was performed using an upright Olympus Provis AX70 microscope, and images were captured with a Nikon DXM1200 digital camera.

Nissl-stained sections at the level of the roof of the lateral ventricle were used to count the callosal septa. The same sections were used to measure the ventral length of the corpus callosum and the dorsal surface of the callosal septa in order to estimate the increase in contact surface between the supporting callosal structures and the CC itself.

The three-dimensional reconstruction of the CS was performed from a single specimen at 22 PCW, using serial sagittal 20-μm-thick sections, 200 μm apart, stained using the Nissl method and digitally scanned. The dorsal surface of the CS and the ventral surface of the CC were outlined from the sagittal sections and were Z-stacked using AutoCAD software.

The postmortem magnetic resonance imaging (MRI) was performed on the brain extracted from the skull with less than 24 h of delay postmortem. A high-field 3.0T MRI device (Magnetom Trio-Tim, Syngo MRB19 software; both by Siemens) was used, with a body surface coil. The T2-weighted TSE sequence consisted of the following parameters: voxel size 0.38 × 0.38 × 1.00, TE 89 ms, TR 13480 ms, acquisition matrix 320 × 320 × 60, number of averages 9, flip angle 120, echo train length 17.

Results

A qualitative analysis of human fetal brain specimens, ranging in age from 16 to 40 PCW, was performed to determine the pattern of CS development in correlation with callosal growth. We aimed to contrast the developmental changes in the septa with the changes in midsagittal area and length of the CC, as well as with its thickness at the level of the genu, isthmus and splenium.

Appearance, morphology and distribution of the callosal septa

The septa are a direct continuation of the subventricular zone (SVZ) and can be viewed morphologically as an integral part of the ventral tier of the CC during human brain development (Jovanov-Milosevic et al. 2006, 2009). Discrete CS are already visible at 16 PCW (not shown). Robust CS are present at 18 PCW and increase in size and number in subsequent weeks (Fig. 1A–F). The septa are best visualized if cross-sectioned along their short axis, which lies radially to the ventral callosal surface. The majority of CS will be cut in such a fashion on parasagittal slices (Fig. 1A–C), where they appear as triangular structures. The septa are not present in the midsagittal plane *per se*, but arise in paramedian slices. Septa increase in size in more lateral planes and reach their full size at the level of the roof of the lateral ventricle (Fig. 1A–C). On coronal slices it is harder to recognize the CS. For example, at the level of the genu they look like horizontal structures arising from

Table 2 Primary antibodies used in the study.

Primary antibodies (clone)	Name or abbreviation (Cat. No.)	Host, isotype	Dilution	Supplier
Anti-Microtubule-Associated Protein-2 (HM2)	MAP2 (M4403)	Mouse, monoclonal, IgG1, affinity purified hybridoma cell culture	1:1000	Sigma-Aldrich, St. Louis, MO, USA
Anti-Microtubule-Associated Protein-1B (clone AA6)	MAP1B (M4528)	Mouse, monoclonal, IgG1, affinity purified hybridoma cell culture	1:1000	Sigma-Aldrich, St. Louis, MO, USA
Anti-synaptophysin (SY38)	synaptophysin (M0776)	Mouse, monoclonal IgG1 kappa, cell culture supernatant	1:100	Dako, Glostrup, Denmark, EU
Anti- synaptosomal-associated protein 25 (SMI81)	SNAP25 (836301)	Mouse monoclonal IgG1, kappa, affinity purified hybridoma cell culture	1: 1000	Biolegend, San Diego, CA, USA
Growth associated protein -43	GAP43 (NB300-143)	Rabbit polyclonal affinity purified IgG	1:1000	Novus Biologicals, LLC, Centennial, CO, USA
Anti-neogenin (N-19)	neogenin (sc-6537)	Goat polyclonal affinity purified IgG	1:200	Santa Cruz, Biotechnology, Inc. Dallas, TX, USA
Anti-ephrinA4 (P-20)	ephrinA4 (sc-912)	Rabbit polyclonal affinited purified IgG	1:200	Santa Cruz, Biotechnology, Inc. Dallas, TX, USA
Anti-human fibronectin	fibronectin (F3648)	Rabbit polyclonal, affinity purified antibody	1:400	Sigma-Aldrich, St. Louis, MO, USA
Anti-Glial Fibrillary Acidic Protein	GFAP (Z0334)	Rabbit, polyclonal purified immunoglobulin	1:1000	Dako Glostrup, Denmark, EU
Anti-human CD68 (514H12)	CD68 (MCA1815)	Mouse, monoclonal IgG2a, tissue Culture Supernatant	1:80	Bio-Rad Antibodies Kidlington, Oxford, UK

the medial wall of the lateral ventricles (Fig. 1D), whereas the coronal slices at more posterior levels will not consistently show the CS. When they are visualized at these levels, they appear as triangular protuberances of SCZ into the ventral tier of CC (Fig. 1F), which can easily be overlooked. At 18 PCW, thin extensions are seen arising from CS. We named these septal tufts (ST) (Figs 1B–F, 2D,E and 3A–C,E,F). These radial extensions of the CS consist of one to a few cellular processes per individual tuft, which protrude and lie between the callosal fibres. The number of ST per single CS varies greatly in a single specimen, and across gestational ages.

It is important to note that the level of the roof of the lateral ventricle is not present in the same parasagittal slice throughout the fronto-occipital extent of the corpus callosum because of the shape of the lateral ventricles. As a result, a parasagittal slice that cuts through the roof of the frontal horn of the lateral ventricle and forceps minor of the callosal radiation will cut laterally to the roof of the body of the ventricle and callosal radiation, and more medially of the occipital horn of the lateral ventricle and the forceps major of the callosal radiation. Thus, to grasp fully the morphology and distribution of septa at a certain developmental stage, serial parasagittal slices must be analysed. Two areas do not follow the general medial-to-lateral gradient of septal prominence: the first is located anteriorly above the glial wedge and the second is situated above the septohippocampal nucleus in the midgestational period (Fig. 2D,E). The nucleus is described in detail by Kostovic et al. (2002); *septo* here refers to the septal region of the diencephalon.

Developmental maximum of the callosal septa

The size of the CS increases during the second half of gestation. The CS reach their maximum at 20 PCW and remain prominent until 26 PCW (Fig. 2A). A 3D reconstruction of the CS (Fig. 2B) shows their morphology during the developmental maximum at 22 PCW. No septa are present in the midsagittal plane and the corpus callosum is flanked ventrally only by the SCZ. Moving laterally, individual septa start to appear and morph into larger, more pronounced structures. The number and size of the septa increase dramatically toward the roof of the lateral ventricle. During their developmental maximum, there are 25–30 septa along with the rostro-caudal extent of the callosal radiation (Fig. 2B). Due to the presence and shape of the CS, the contact surface between supporting structure on one side and the growing callosal fibre radiation on the other, is enlarged. When measured during their developmental maximum, the contact surface is increased up to 2.5-fold.

During this period the CS can be visualized by postmortem MRI. Septa are visible as hypointense areas within the ventral tier of the CC on T2 MRI scans at 22 PCW (Fig. 2C). The septa were clearly seen only at the level of the roof of the body of the lateral ventricle. We were not

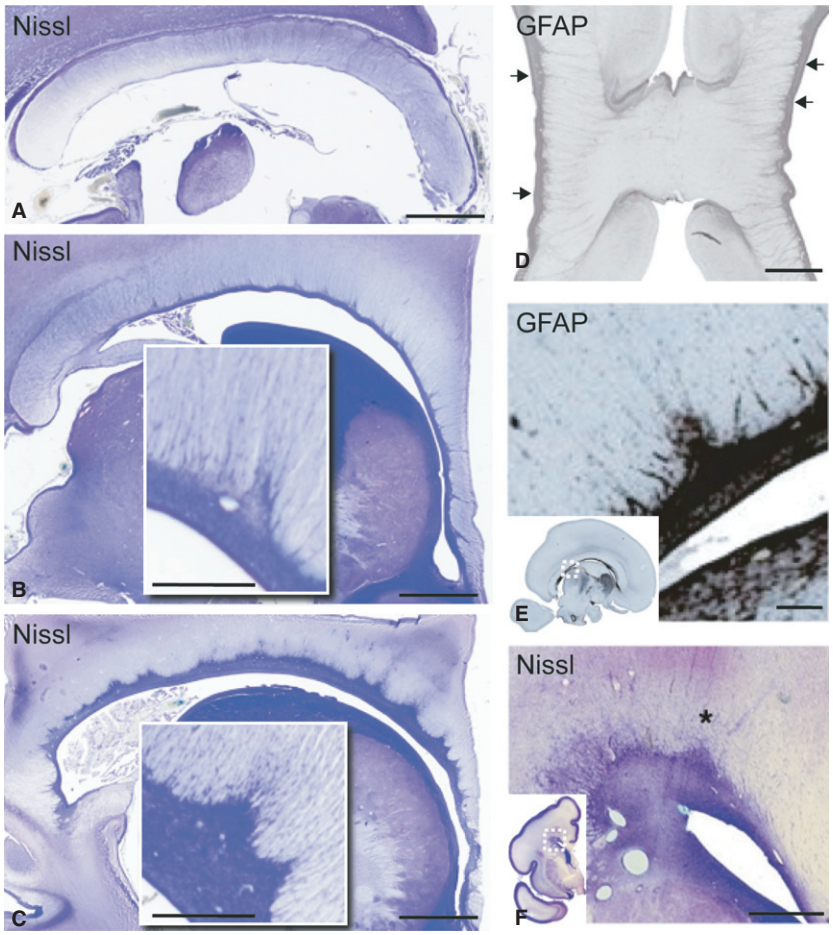

Fig. 1 Sagittal and coronal sections of the corpus callosum and callosal septa during midgestation (22 PCW A–C; 18 PCW D,E; 24 PCW F). The sagittal sections (A–C) show that the callosal septa are not visible at the midline (A), even during their developmental maximum at 22 PCW. The septa increase in their visibility and prominence in paramedian sections (B), and reach their maximum at the level of the roof of the lateral ventricle (C). The inserts in (B) and (C) are high-magnification images of individual septa showing the increase in septal size and cellular density from paramedian towards more lateral levels. Coronal section at the level of the genu (D), and a parasagittal section of the corpus callosum body (E) at 18 PCW stained for GFAP show the glia cell population within the septa. Note the horizontal, linear appearance of septal tufts, arising from individual callosal septa (arrows) and extending through almost the full width of the callosum (D). The sagittal section shows the distribution of GFAP-reactive astroglia in the subcallosal zone and the callosal septa (E). Note the callosal septa in the posterior callosal body, and several septal tufts arising from a single septa (E, insert). Section of fetal brain at 24 PCW stained by the Nissl method (F) shows a coronal view of a cross-section of the callosal septa (asterisk) and tufts at the level of the roof of the lateral ventricle. Scale bars: 2.5 mm (A–C); 1 mm (B,C, inserts D and E), 300 μm (F).

able to identify the septa on all parasagittal slices, presumably secondary to a combination of their size, voxel size used for MR imaging and the angle at which the septa were cut by the MR acquisition matrix.

Cellular and axon guidance components of the callosal septa at the developmental maximum

The callosal septa have a high density of cells, as evidenced by Nissl staining (Figs 1B,C,F, 2A, 3A and 5A). The major cellular component of the CS is a glial fibrillary acidic protein (GFAP)-positive cell population (Figs 1D,E and 3B), which have a similar density throughout the dorsal portion of the SCZ continuum. The vast majority of septa tufts are GFAP-immunoreactive (Figs 1D,E and 3B). Another glial population, microglia, can be seen continuously extending from the SCZ/SVZ into the individual septa with a small portion of cells dispersed within the tufts and within callosal fibre bundles (Fig. 3F). During the septal maximum, microglia, as seen by CD-68 immunoreactivity, are primarily located in the dorsal portion of the SCZ, and to a lesser extent within the CS (Fig. 3F). The extent of the distribution and the cellular density varied between our samples, and we were not able to exclude that this variation was secondary to the specific clinical situation related to miscarriage or premature birth. The cell morphology of microglia also varied between specimens, with the majority displaying a

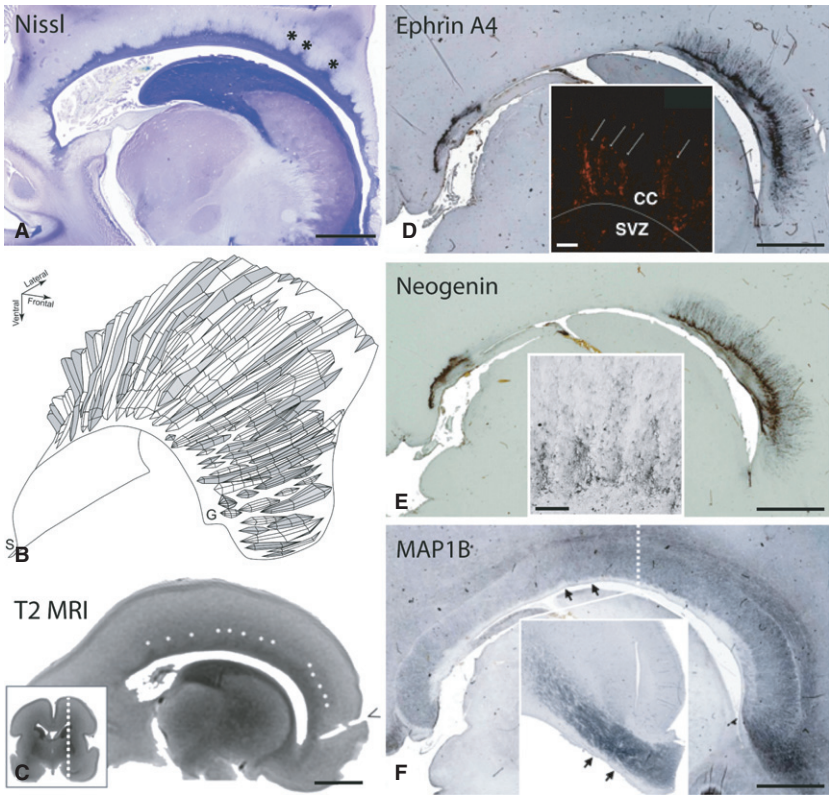

Fig. 2 The corpus callosum and the callosal septa at their developmental maximum. Parasagittal section stained by the Nissl method demonstrates an abundance of callosal septa (*) arising from the subcallosal zone at 22 PCW (A). The 3D reconstruction from the same brain specimen reveals between 25 and 35 individual septa along the rostrocaudal axis at their developmental maximum (view from the frontal aspect, B). Note the lack of septa in the midsagittal plane, their occurrence and increased prominence in more lateral aspects of the callosal radiation, and horizontally oriented septa in the genu of the corpus callosum (B). A T2 MRI scan of an *ex vivo* fetal brain at 22 PCW shows triangular areas of signal hypointensity arising from the ventricular surface, consistent with callosal septa (white asterisks, C). The dashed line in the insert image indicates the level of the parasagittal scan. Both ephrinA4 (D) and neogenin (E) immunoreactivity are primarily located in the septa and their tufts at the interface with the callosal bundle, also showing linear extensions of immunopositivity into the fiber bundle itself (inserts in D and E) and spanning the thickness of the corpus callosum. The expression in the subcallosal zone is much weaker than that of the callosal septa (D,E). Note that the absence of staining at the level of the posterior body of the callosum is due to a combination of the lateral level of the parasagittal slice and a narrow mediolateral band of distribution of guidance molecules. Immunohistochemical stain for MAP1B (F) denotes the distribution of phosphorylated microtubule-associated protein, indicating growth of the callosal fiber bundle. MAP1B immunoreactivity nicely outlines the shape of the callosal septa and the subcallosal zone, neither of which is MAP1B-immunoreactive (arrows, F). The insert shows the same pattern of MAP1B distribution at paramedian levels on the coronal section from the opposite hemisphere at the level of the midbody (dashed line, F). T2 MRI, T2-weighted magnetic resonance imaging; S, splenium; G, genu; CC, corpus callosum; SVZ, subventricular zone. Scale bars: 5 mm (A–F and insert in F), 100 μm (inserts D and E).

rounded morphology, whereas others were ramified. The distribution of neurons as evidenced by MAP2 immunoreactivity was restricted to the upper portions of the CS (Fig. 3C), which is consistent with our previous findings that showed NeuN-positive neurons in the same location (Jovanov-Milosevic et al. 2006). A small part of tufts are also positive for MAP2, a marker of neuronal soma and dendrites (Fig. 3C).

The guidance molecules ephrinA4 and neogenin are expressed during midgestation in CS with similar distributions (Fig. 2D,E). They are primarily located at the interface of the CS and the callosal bundle. Fine immunoreactivity for axon guidance cues extends between the callosal fibres and spans almost the full thickness of the callosum (Fig. 2D,E, inserts), indicating their involvement in growing callosal axons. Indeed, MAP1b immunoreactivity, which stains for growing axons (for review see Yang et al. 2012) was distributed through the full thickness of the callosum in the paramedian slides at this time-period (Fig. 2F). We confirmed this observation with synaptosomal associated protein (SNAP25, Fig. 3D), synaptophysin (Fig. 5B) and growth-associated protein 43 (GAP43, Fig. 5C), all of which are well-established markers for growing axons (Osen-Sand et al. 1993; Eastwood et al. 1994). These findings support the idea that during human midgestation, axonal ingrowth occurs throughout the entire rostro-caudal and dorso-

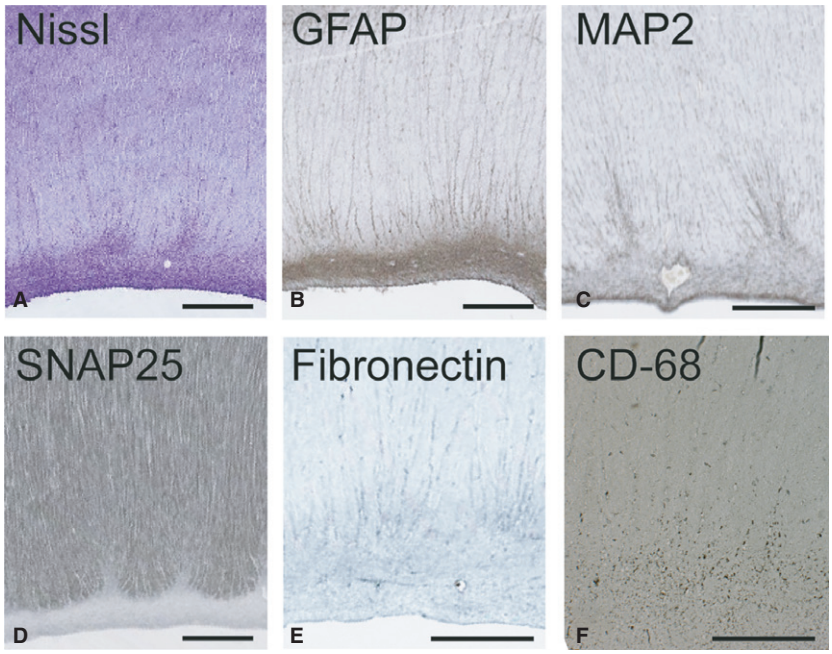

Fig. 3 High-resolution microphotographs of callosal septa demonstrate their cellular and extracellular content during their developmental prominence at 23 PCW. Staining by the Nissl method (A) and GFAP-immunoreactivity (B) both show a similar distribution of cell bodies. GFAP distribution also extends into the septal tufts intimately contacting the smaller callosal bundles. Microtubule-associated protein-2 (MAP2) immunoreactivity in the dorsal aspects of the callosal septa confirms the presence of neurons in the septa whose processes extend into septal tufts (C). The SNAP25 immunoreactivity restricted to callosal bundles shows that callosal axons grow, and that they avoid and do not invade septa at this developmental stage (D). Extracellular expression of fibronectin is distributed in the ventral-most bundles of the callosum, and their interface with the callosal septa/subcallosal zone (E). CD68 immunoreactivity shows microglial distribution located primarily within the subcallosal zone and to a lesser extent within the septa. Scattered CD68-positive cells are visible within the fiber bundle. Scale bars: 1 mm.

ventral extent of the CC. As mentioned above, the CS increase the contact surface between the fibre bundles and supporting structures, so that the accumulation of guidance molecules or growth-promoting ECM molecules in the CS and at this interface will be able to optimize their influence on the ingrowing axons. The overall distribution pattern of the growth-promoting extracellular fibronectin is similar to that of the guidance molecules, although less restricted (Fig. 3E). A schematic view of the distribution of cell populations and guidance molecules in the CS during their developmental maximum is summarized in Fig. 4.

Resolution of the callosal septa

A gradual resolution of CS occurs after midgestation, as evidenced by a steady decrease in septal size and number (Fig. 4A,D). Compared with the previous time-period (Fig. 5A–C), a significant change in the pattern of staining for synaptophysin and GAP43 was observed at 33 PCW (Fig. 5E,F). Immunoreactivity to synaptophysin and GAP43 slowly decreases, and becomes progressively more restricted – initially to the ventral third of the CC, then to the CS and the SCZ. These findings indicate that the ingrowth of callosal axons is restricted to the ventral portion of the CC and that they invade the CS, possibly contributing to their resolution. At term, the CS are greatly reduced in size and number.

Relationship between the callosal septa and the growth of the corpus callosum

To see how the changes in the CS relate to the growth of the corpus callosum, we measured the midsagittal callosal area and the thicknesses of the callosal genu, isthmus and splenium (Fig. 6). An important detail to emphasize is that all measurements of the callosum were obtained in the midsagittal plane, where there are no CS; thus, their presence would not confound the measurements. Our samples showed three phases of callosal midsagittal area growth: (1) an initial linear increase up to 27 PCW followed by (2) a plateau lasting until 33 PCW, and finally (3) a resumption of linear growth (Fig. 6, top graph, black dots). The anterior–posterior length of the callosum showed continuous growth during the second half of gestation (Fig. 6, top graph, white dots). During the same time-period, the genu showed a linear increase in its thickness, whereas the isthmus and splenium did not (Fig. 6, bottom graph). Throughout development, the isthmus remained the thinnest segment of the corpus callosum. The initial growth of the CC midsagittal area coincides with the developmental

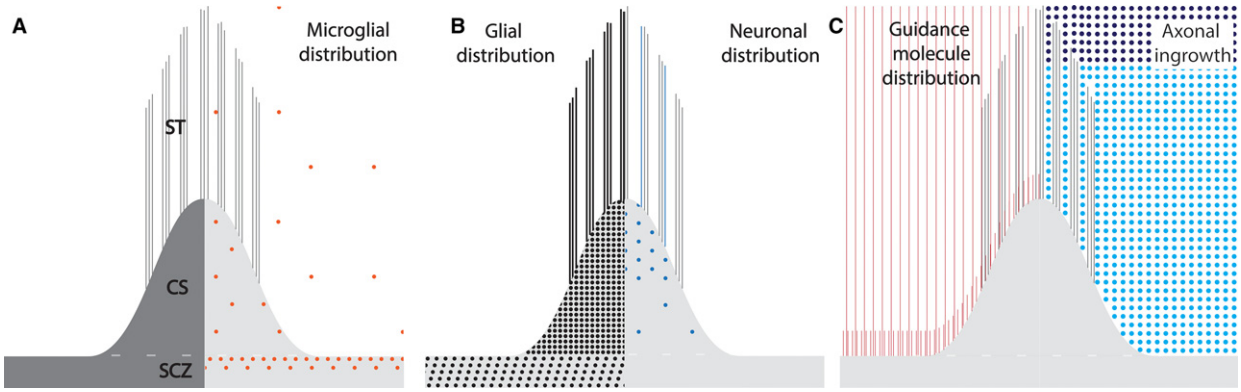

Fig. 4 Schematic representation of the callosal septa in the sagittal plane with the distribution of different cell populations and axonal guidance cues, at their developmental maximum. Callosal septa (CS) arise from the subcallosal zone (SCZ), ending within the callosal fibre bundle as septal tufts (ST) (A, left). Distribution of microglia as seen by CD68 immunostaining (A, right). Microglia are located at a high density in the upper portion of the subcallosal zone, and with lesser density through the full extent of the septa. Scattered microglia are also present in the callosal fibre bundle at the interface with the CS/SCZ. GFAP-positive cells make up the major cellular population within the septa, with GFAP-positivity extending into the septal tufts (B, left). Neuronal distribution as seen by MAP2 immunostaining (B, right) is highest in the upper portion of the septa. Occasional septal tufts also contain MAP2-positive processes. The distribution of the guidance molecules, ephrinA4 and neogenin (and semaphorin3A, see Judaš et al. 2005), is primarily located within the septa and within the callosal fibre bundle at the interface between the two (C, left). Note that the distribution of the axon guidance molecules extends beyond the septa and septal tufts into the callosal fibre bundle (C, left). Distribution of ingrowing axons (light blue), based on the expression of GAP-43, SNAP-25 and synaptophysin (C, right). They do not invade the septa during the period of the developmental maximum of the septa.

maximum of the CC, whereas the plateau of midsagittal area growth occurs during the ongoing resolution of the CS.

Discussion

We propose that the CS are paramedian guideposts for growing callosal axons. Together with the SCZ, they form a thick zone (like a thick quilt), with creases and furrows on its dorsal side that become more prominent toward its lateral sides (Fig. 2B). The corpus callosum lies on this quilt, stretched between the roofs of the lateral ventricles. The CS were first described by our group (Jovanov-Milosevic et al. 2006). However, they are visible in the sagittal images of other publications as small triangular dorsal extensions of the glioepithelium (described as mounds of migrating cells in Bayer & Altman, 2005) or as irregularities of the ventral surface of the callosal body (Lent et al. 2005). They have not been described in further detail, probably because they are transient and difficult to appreciate on coronal sections.

Guidance cues in the callosal septa

The expression of ephrinA4 and neogenin, as presented here, is restricted to the callosal septa and tufts, in a fairly narrow paramedian fashion that extends through the rostro-caudal axis of the callosal fibre system, and partially overlies the septohippocampal nucleus. We propose that the accumulation of guidance molecules in the paramedian aspects of the callosal radiation might offer a unique opportunity to affect axonal populations differentially, depending on their medio-lateral location (for a review of the development of cortical connections, see Kostovic & Jovanov-Milosevic, 2006). The expression pattern of guidance cues over the septohippocampal nucleus may be important for the separation of callosal fibres from the fornix system based on the differential expression of receptors on growing callosal and fornical axons, thus preventing callosal axons from entering the fornix system and *vice versa*. The ephrins/EphRTK family members are known to be short-range, membrane-bound guidance cues, with repulsive cell–cell interaction (Klein 2004; Mendes et al. 2006; Nishikimi et al. 2013). This system also has a crucial role in the compartmentalization of the striatum in the rat, by delineating the matrix from striosomes, and the segregation of neocortical from limbic striatal inputs (Janis et al. 1999). The expression of ephrinA4 in the subventricular region demonstrated in the mouse (Mendes et al. 2006) is consistent with our data that show ephrinA4 in the CS/SCZ at the interface with the growing corpus callosum. Neogenin has been shown in the murine callosal radiation (Van den Heuvel et al. 2013), exerting both repellant and attractant effects on growing axons in the vertebrate forebrain, depending on interactions with either netrin-1 or repulsive guidance molecules (RGM), respectively (Wilson & Key, 2006).

The guidance of axons or migrating cells is moderated by extracellular matrix molecules, such as heparan- and chondroitin-sulphate, either through their direct effect on the

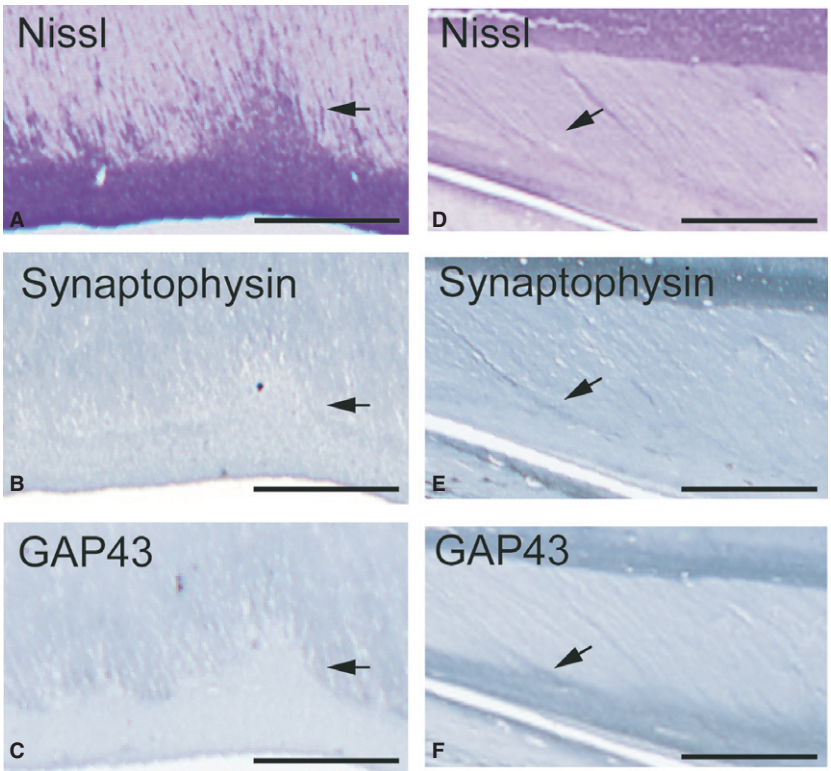

Fig. 5 To contrast the developmental maximum with the resolution of the septa, adjacent sections through the level of the callosal midbody septa were stained by the Nissl method (A,D), synaptophysin (B,E) and growth-associated protein-43 (GAP43) (C,F) immunohistochemistry, at 20 PCW (A–C) and 33 PCW (D-F). Arrows point to the callosal septa. During the septal maximum, both synaptophysin and GAP43 immunoreactivity are confined within growing callosal axons and neither shows any immunoreactivity in any part of the septa (B,C). At 33 PCW, synaptophysin is expressed lightly within the tops of the septa, whereas GAP43-immunopositivity is located through the full extent of the septa and partially in the subcallosal zone, indicating that the growing axons invade the septa, presumably leading to their resolution. Scale bars: 0.5 mm in (A–C) and 1 mm in (D,F).

growth cones (Yang et al. 2006) or through their interaction with and modification of the function of guidance molecules (Lindwall et al. 2007). For example, the heparan-sulphate proteoglycans mediate the attractive effects of Sema5A, whereas the chondroitin-sulphate proteoglycans convert the Sema5A function into an inhibitory one (Kantor et al. 2004). The fibronectin expression presented here, is distributed diffusely in a band-like fashion in the ventral tier of the CC and upper CS, indicating a permissive area for callosal axonal growth. Fibronectin might work in collaboration with chondroitin-sulphate, previously shown to be located in the CS and the upper portion of the SCZ (Jovanov-Milosevic et al. 2006), which forms a hostile border preventing axons from invading the CS during midgestation. To explore further the significance of ephrinA4 and neogenin in human callosal development, the expression pattern of their receptors and ECM partners will need to be examined. Their roles as callosal axonal attractants or repellents will remain unclear until the distribution and relative relationships of receptor-ligand pairs and ECM modulators are followed throughout development.

Cellular composition of the septa

The cellular composition of CS with tufts is not dissimilar to earlier midline guideposts, such as the glial wedge or midline sling (Ren et al. 2006; Donahoo & Richards, 2009). The major cellular population in the CS are glia (GFAP-positive), with glial bodies forming the base and glial processes extending into tufts. The tufts themselves consist mainly of cellular processes, the majority of which are GFAP-positive. Our data show that microglia are also present in the septa, distributed within the SCZ at the ventral surface of the growing callosum and, to a far lesser extent, within the callosal fibre bundle itself. The association of microglia with growing axonal tracts is a known phenomenon (Verney et al. 2010). Initially thought to be primarily important for clearing a path for developing axons (Valentino & Jones, 1982) and phagocytosis of exuberant axons during the pruning phase of axonal tract development (Innocenti et al. 1983), microglia have been shown to have a promoting function for neurite development, but do not seem to be crucial for the midline crossing of callosal axons (Pont-Lezica et al. 2014). Studies that have shown two microglial populations associated with callosal development – round microglia with a high expression of CD-68 that accumulates around the fibre tract, and ramified microglia found within the growing callosal tract (Pont-Lezica et al. 2014) – are consistent with our findings. A smaller portion of the CS comprises neurons. The presence of a transient neuronal population in midline structures has been recognized in studies of early CC development (Shu et al. 2003; Niquille et al. 2009). We have shown MAP2-immunoreactive processes located at the top of individual CS, where NeuN neurons were previously described (Jovanov-Milosevic et al. 2006). They might provide guidance to axons and/or migrating cells, similar to the role of the midline sling (Shu et al. 2003). The role

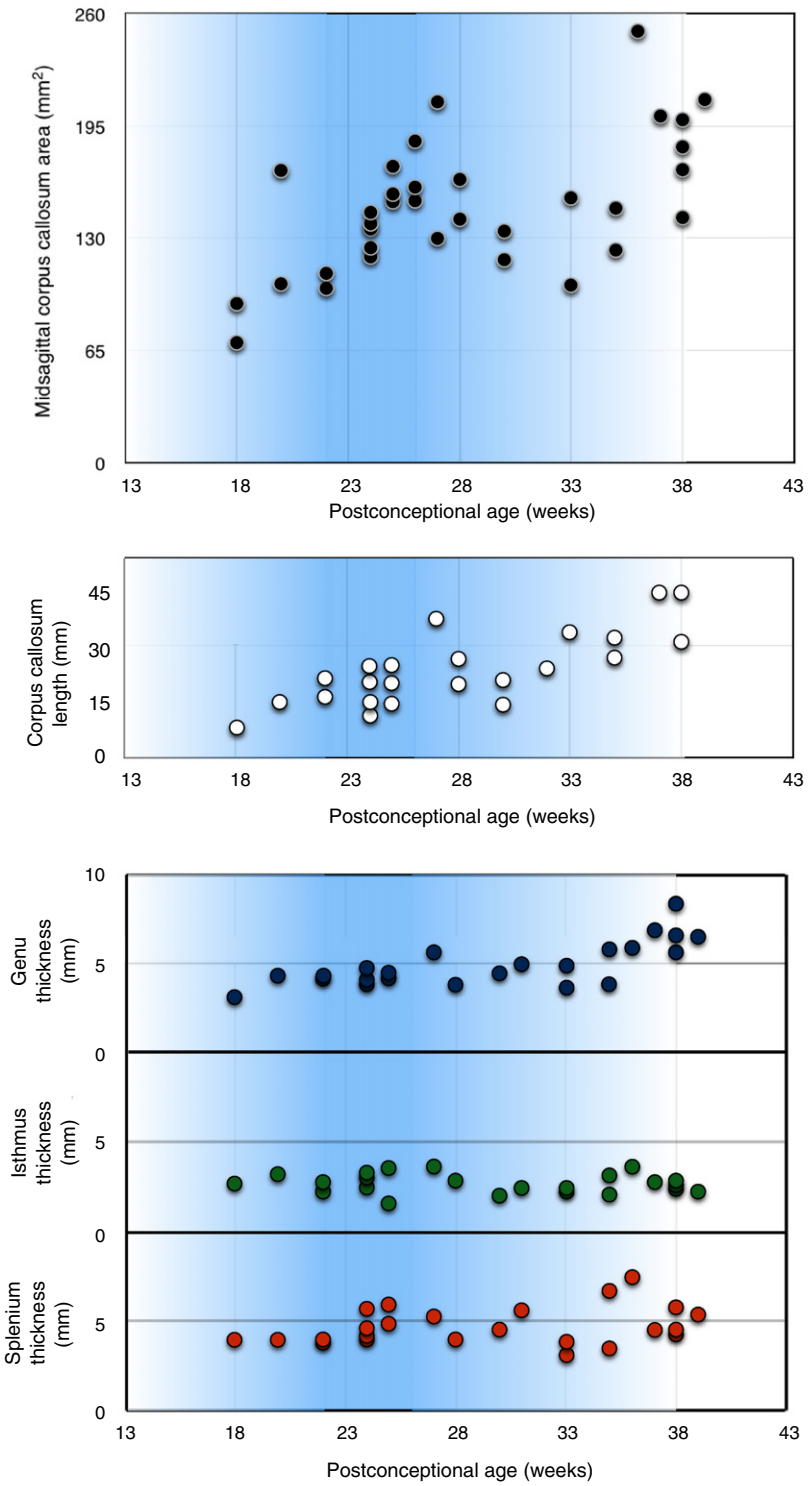

Fig. 6 Midsagittal callosal area from 18 to 40 PCW (black circles in the top graph) shows an increase from 18 to 26 PCW, overlapping with the developmental maximum of callosal septa (20–26 PCW), followed by a plateau of the callosal midsagittal area between 27 and 33 PCW, after which the corpus callosum resumes its growth. The length of the corpus callosum in the midsagittal plane (linear distance from the most anterior to the most posterior point of the corpus callosum (white circles in the graph in the middle) from 18 to 40 PCW reveals a continuous increase with no growth plateau. Changes in the thickness (length of the radial axis perpendicular to the ventral surface of the callosum, in the midsagittal plane) of the genu (blue), isthmus (green) and splenium (orange) from 18 to 40 PCW (bottom graph) demonstrate a continuous growth of the genu throughout the studied period, whereas the thickness of the isthmus and splenium stagnates. The intensity of the blue-shaded background in the intensity of the blue-shaded background in the graphs represents the prominence of the callosal septa, graphs represents the prominence of the callosal septa, with their maximum occurring between 20 and 26 PCW.

of transient neuronal populations in axonal pathfinding has been shown for thalamo-cortical pathways, the lateral olfactory tract and the optic chiasm (Sretavan et al. 1995 Sato et al. 1998; Lopez-Bendito et al. 2006). Gamma-aminobutyric acid (GABA)ergic and glutamatergic cell populations have been shown to provide chemoattractant cues for callosal axons (Niquille et al. 2009), which further supports the involvement of CS neurons in guidance.

Thus, we propose that, based on their location, shape, cellular and molecular composition, CS and ST can be

considered specialized transient structures that serve to support, guide and segregate some growing callosal fibre populations while uniting others, between the midline and the roof of the lateral ventricles, in the second half of human gestation.

Callosal septa revealed by MRI

We also report here that the callosal septa are visualized on fetal *ex vivo* 3T MRI as triangular hypointesities, located in the CC at the roof of the lateral ventricles during their developmental maximum. This feature of fetal MR images is dissimilar to the recently published foliate structure in the corpus callosum of adults visualized by *in vivo* 7T MRI (Wiggins et al. 2007) , which is related to the indusium griseum (IG), and resembles in size, shape and distribution the glial architecture of the mature corpus callosum.

Relationship of the callosal septa and corpus callosum growth

During the early period of septal presence and during their maximum expansion (20–26 PCW), the majority of the newly arrived callosal axons are 'follower' axons guided by the already present callosal bundles. Our data show that markers of axon growth and elongation, such as MAP1b and SNAP-25, are strongly expressed through the full thickness of the corpus callosum during this time-period, indicating that the axon growth is diffusely distributed throughout the callosal width. Later in gestation, this diffuse distribution of axonal growth markers becomes confined to the ventral portions of the callosum. At 33 PCW the expression patterns of GAP-43 and synaptophysin are restricted to a narrow band in the ventral aspects of the corpus callosum, suggesting that the later-arriving axons are added primarily in the ventral portion of the callosum. This finding of restriction of callosal axonal ingrowth to more ventral aspects of the human callosum during a later period of gestation is consistent with findings in animal models and previous studies in humans (Ozaki & Wahlsten, 1992; De Benedictis et al. 2016).

In terms of morphological measurements, our data show that initial midsagittal area growth of the corpus callosum coincides with the developmental maximum of callosal septa, whereas the midsagittal area growth plateau coincides with the gradual resolution of the septa between approximately 27 and 33 PCW. A previous study on the postmortem human CC (Clarke et al. 1989), along with those on cat and Rhesus monkey (Berbel & Innocenti, 1988; Lamantia & Rakic, 1990; LaMantia & Rakic, 1990) have shown a similar growth pattern of the CC. Some clinical studies of human callosal growth utilizing ultrasound and MRI have also noted a non-linear increase in callosal length (Harreld et al. 2011; Araujo et al. 2012). In 2001, Achiron & Achiron described a linear increase of callosal length of between 14 and 36 PCW, using linear regression, but the data point scatter of callosal length supports, if not an actual plateau, at least represents a slowing of the rate of linear growth around 28 PCW. Another study, assessing the relationship between the corpus callosum area and cognitive and motor outcomes, showed that, in control subjects, the corpus callosum midsagittal area size remained unchanged between the group of 26–28 PCW and the group 35–38 PCW (Wu et al. 2018). We are not able to discuss the change in axonal number in the midsagittal callosal area based on the changes in our sample. Electron microscopy studies of axonal number estimate that the adult human corpus callosum consists of 200–300 million axons (Aboitiz et al. 1992; Aboitiz & Montiel, 2003). Studies on cats (Fleishhauer & Schlueter, 1970; Berbel & Innocenti, 1988) and Rhesus monkeys (LaMantia & Rakic, 1990a,b; for review see Innocenti & Price, 2005) show extreme axonal overproduction during fetal callosum development, followed by a dramatic decrease in axonal number. Although it is tempting to try to infer these processes and the number of callosal axons based on callosal midsagittal surface size, this approach is not appropriate. Axonal diameter varies depending on axonal maturation course and its origin. The decrease in the callosal midsagittal area occurs at the same time as the decrease in axonal number in the cat brain (Berbel & Innocenti, 1988) but in Rhesus monkeys the decrease in callosal axonal number occurs after the plateau of the midsagittal callosal area, immediately prior to birth (LaMantia & Rakic, 1990), which suggests the existence of species differences and/or methodological challenges.

Detailed studies of callosal topography in primates have shown a rostro-caudal distribution of axons depending on their region of origin. For example, frontal regions in Rhesus monkeys connect through the genu, whereas motor areas connect through the anterior callosal body (Karol & Pandya, 1971; Pandya et al. 1971; Seltzer & Pandya, 1983; Barbas & Pandya, 1984; Cipolloni & Pandya, 1985; Rockland & Pandya, 1986; Hofer & Frahm, 2006; Hofer et al. 2008). The dorso-ventral topographical distribution of callosal axons has been shown in rodents (Ozaki & Wahlsten, 1992; Richards et al. 2004), cats (Matsunami et al. 1994) and humans (Dougherty et al. 2007; Tovar-Moll et al. 2007). A notable finding is that the axons that connect the frontal lobes in humans extend more caudally into the posterior body of the callosum (De Benedictis et al. 2016), presumably secondary to the expansion of the frontal cortical areas. In our study sample, only the genu showed an increase in thickness throughout the second half of gestation. Taking this finding into account, together with the data on topography from other studies of callosal growth by segments (Clarke et al. 1989; Denenberg et al. 1991; Peters et al. 2000), we can infer that the frontal lobe regions undergo a period of increasing interhemispheral connectivity toward term age. It is reasonable to assume that the genu growth involves an increase in the number of

frontal lobe axons, an increase in their diameter or both, as myelination would not contribute to the increase in the size of the genu during the second half of human gestation, as this begins around term-equivalent age (Luttenberg, 1966). Another interesting observation is that *in utero* fetal brain MRI tractography has revealed an adult-like pattern of callosal topography that is already established by 28 PCW (Kasprian et al. 2008; Zanin et al. 2011), which could mean that CS might be involved in the establishment of axonal topography.

Limitations of the study

Although the number of brain specimens used in this study is sufficient for a descriptive anatomical aspect of the study, it is insufficient to draw firm quantitative conclusions. However, we do believe that the measurements of callosal growth emphasize that the midsagittal area needs to be viewed from the perspective of a changing, not a constant, growth rate. The analysis of the size of the midsagittal area of the corpus callosum is potentially confounded by varying degrees of tissue shrinkage during the fixation process, as samples at earlier gestational ages are higher in water content, which would increase the degree of tissue shrinkage in these specimens. However, as there is no evidence that the corpus callosum in the midsagittal plane is inherently different in terms of constituents between 20 and 35 PCW of human gestation (and in equivalent ages in animal models), it is likely that the observed plateau is a true finding.

All specimens analysed in our study were obtained after spontaneous abortions or immediate demise of prematurely born infants. As such, we cannot consider them to be fully representative of normal prenatal development. Premature birth itself is associated with a high incidence of amniotic inflammation and infection (Oh et al. 2017). These states lead to a fetal inflammatory response (Romero et al. 2016) and have been shown to alter the metabolic profiles in fetal and neonatal brains (Brown et al. 2017). The activity of microglia is affected by the maternal immune system and could be activated by a pro-inflammatory fetal state (Boksa, 2010; Prins et al. 2018), leading to an increase in microglial cell number and distribution, as well as their altered morphology. We aimed to limit this effect by selecting samples with no macro- or micro-morphological anomalies, and only fetuses and premature infants with normal prenatal courses up to abortion or premature birth.

Conclusion

The strategic location, shape, cellular composition and presence of axon guidance molecules establish the CS as guidepost structures in the CC development during the second half of human gestation. The CS are involved in guiding callosal axons toward the midline and, after midline-crossing, toward the intermediate zone of their designated cortical regions. Most likely, this is achieved by sorting of axons from different cortical regions and areas, into accurate position or fascicles within the callosal radiation (and consequently correct position in the callosal body), on the basis of interactions of guidepost ligands and axonal receptors. On the contralateral side, the CS possibly route callosal axons on the correct path directed to the targeted cortical region. This idea is even more plausible considering the time-period at which callosal septa are present – during establishment of the topography of callosal connections. On one hand, the maximum of CS development overlaps with the significant growth of the cortical plate and presumed increase in number of callosal axons (especially from the prefrontal regions), as well as with the increase in midsagittal area of the corpus callosum. On the other hand, CS resolution coincides with the midsagittal area growth plateau and ends after the adult-like topography of the callosal fibres has been established. Future research directions should include characterization of the guidance ligand-receptor partners and their ECM modulators, including the changes in expression levels and locations with advancing gestational age. The colocalization of guidance molecules with glial, neuronal or microglial markers would further clarify the role of different cell populations in the growth of CC. An additional role of CS is that they may provide a path through the thick callosal bundles for late radially migrating progenitors of neurons and glial cells. For a structure to be clinically relevant, it needs to be amenable to visualization by modern imaging methods in a live patient. We showed that the CS can be imaged using *ex vivo* T2-weighted 3T MRI. The next research steps should include an evaluation of *in utero* fetal imaging and imaging data obtained in extremely premature infants early in their postnatal courses. Due to the combination of a high cellular density and the presence of extracellular matrix in the CS, these structures would have a diffusion signal distinct from the compact callosal bundles, and their evaluation could be used as one of the indicators of normal vs. abnormal corpus callosum development.

Acknowledgements

This publication was co-financed by the Scientific Centre of Excellence for Basic, Clinical and Translational Neuroscience (project 'Experimental and clinical research of hypoxic-ischemic damage in perinatal and adult brain'; GA KK01.1.1.01.0007 funded by the European Union through the European Regional Development Fund), and UniZg BM0054 and Adris Fund (HIMRICO). We thank Dr Davor Petrovic and his colleagues from the Department of Health of Women and Family Hospital of the University Hospital Center of Zagreb for co-operation in collecting human brain samples, and B. Popovic, M. Horvat and D. Budinscak for excellent technical support.

Conflict of interest

The authors have no conflict of interest to declare.

Author contributions

M.C. performed measurements of the corpus callosum, *ex vivo* MRI imaging, and rendered schematic representations of callosal septa. N.J.M. developed the study design and immunohistochemical protocols. Both authors analysed and interpreted the histological data and the results, wrote and critically revised the article, and approved it for submission.

References

Aboitiz F, Montiel J (2003) One hundred million years of interhemispheric communication: the history of the corpus callosum. *Braz J Med Biol Res* **36**(4), 409–420.

Aboitiz F, Scheibel AB, Fisher RS, et al. (1992) Fiber composition of the human corpus callosum. *Brain Res* **598**(1–2), 143–153.

Achiron R, Achiron A (2001) Development of the human fetal corpus callosum: a high-resolution, cross-sectional sonographic study. *Ultrasound Obstet Gynecol* **18**(4), 343–347.

Araujo Junior E, Visentainer M, Simioni C, et al. (2012) Reference values for the length and area of the fetal corpus callosum on 3-dimensional sonography using the transfrontal view. *J Ultrasound Med* **31**(2), 205–212.

deAzevedo LC, Hedin-Pereira C, Lent R (1997) Callosal neurons in the cingulate cortical plate and subplate of human fetuses. *J Comp Neurol* **386**(1), 60–70.

Barbas H, Pandya DN (1984) Topography of commissural fibers of the prefrontal cortex in the rhesus monkey. *Exp Brain Res* **55**(1), 187–191.

Bayer SA, Altman J (2005) *Atlas of Human Central Nervous System Development*. Boca Raton: Taylor and Francis Group, CRC Press.

Berbel P, Innocenti GM (1988) The development of the corpus callosum in cats: a light- and electron-microscopic study. *J Comp Neurol* **276**(1), 132–156.

Boksa P (2010) Effects of prenatal infection on brain development and behavior: a review of findings from animal models. *Brain Behav Immun* **24**(6), 881–897.

Brown AG, Tulina NM, Barila GO, et al. (2017) Exposure to intrauterine inflammation alters metabolomic profiles in the amniotic fluid, fetal and neonatal brain in the mouse. *PLoS ONE* **12**(10), e0186656.

Caminiti R, Ghaziri H, Galuske R, et al. (2009) Evolution amplified processing with temporally dispersed slow neuronal connectivity in primates. *Proc Natl Acad Sci U S A* **106**(46), 19551–19556.

Cipolloni PB, Pandya DN (1985) Topography and trajectories of commissural fibers of the superior temporal region in the rhesus monkey. *Exp Brain Res* **57**(2), 381–389.

Clarke S, Kraftsik R, Van der Loos H, et al. (1989) Forms and measures of adult and developing human corpus callosum: is there sexual dimorphism? *J Comp Neurol* **280**(2), 213–230.

De Benedictis A, Petit L, Descoteaux M, et al. (2016) New insights in the homotopic and heterotopic connectivity of the frontal portion of the human corpus callosum revealed by microdissection and diffusion tractography. *Hum Brain Map* **37**(12), 4718–4735.

Denenberg VH, Cowell PE, Fitch RH, et al. (1991) Corpus callosum: multiple parameter measurements in rodents and humans. *Physiol Behav* **49**(3), 433–437.

Donahoo AL, Richards LJ (2009) Understanding the mechanisms of callosal development through the use of transgenic mouse models. *Semin Pediatr Neurol* **16**(3), 127–142.

Dougherty RF, Ben-Shachar M, Deutsch GK, et al. (2007) Temporal-callosal pathway diffusivity predicts phonological skills in children. *Proc Natl Acad Sci U S A* **104**(20), 8556–8561.

Eastwood SL, Burnet PW, McDonald B, et al. (1994) Synaptophysin gene expression in human brain: a quantitative in situ hybridization and immunocytochemical study. *Neuroscience* **59**(4), 881–892.

Edwards TJ, Sherr EH, Barkovich AJ, et al. (2014) Clinical, genetic and imaging findings identify new causes for corpus callosum development syndromes. *Brain* **137**(Pt 6), 1579–1613.

Fame RM, MacDonald JL, Macklis JD (2011) Development, specification, and diversity of callosal projection neurons. *Trends Neurosci* **34**, 41–50.

Fleishhauer K, Schlueter G (1970) Ueber das posnatale Wachstum des Corpus Callosum der Katze (Felis domestica). *Z Anat Entwick Gesch* **132**, 228–239.

Gazzaniga MS (2000) Cerebral specialization and interhemispheric communication: does the corpus callosum enable the human condition? *Brain* **123**(Pt 7), 1293–1326.

Harreld JH, Bhore R, Chason DP, et al. (2011) Corpus callosum length by gestational age as evaluated by fetal MR imaging. *AJNR Am J Neuroradiol* **32**(3), 490–494.

Hedreen JC, Yin TC (1981) Homotopic and heterotopic callosal afferents of caudal inferior parietal lobule in *Macaca mulatta*. *J Comp Neurol* **197**(4), 605–621.

Hofer S, Frahm J (2006) Topography of the human corpus callosum revisited: comprehensive fiber tractography using diffusion tensor magnetic resonance imaging. *NeuroImage* **32**, 989–994.

Hofer S, Merboldt KD, Tammer R, et al. (2008) Rhesus monkey and humans share a similar topography of the corpus callosum as revealed by diffusion tensor MRI *in vivo*. *Cereb Cortex* **19**, 1079–1084.

Huang H, Xue R, Zhang J, et al. (2009) Anatomical characterization of human fetal brain development with diffusion tensor magnetic resonance imaging. *J Neurosci* **29**(13), 4263–4273.

Innocenti GM, Price DJ (2005) Exuberance in the development of cortical networks. *Nat Rev Neurosci* **6**, 955–965.

Innocenti GM, Clarke S, Koppel H (1983) Transitory macrophages in the white matter of the developing visual cortex. II. Development and relations with axonal pathways. *Brain Res* **313**(1), 55–66.

Innocenti GM, Ansermet F, Parnas J (2003) Schizophrenia, neurodevelopment and corpus callosum. *Mol Psychiatry* **8**(3), 261–274.

Janis LS, Cassidy RM, Kromer LF (1999) Ephrin-A binding and EphA receptor expression delineate the matrix compartment of the striatum. *J Neurosci* **19**(12), 4962–4971.

Jovanov-Milosevic N, Benjak V, Kostovic I (2006) Transient cellular structures in developing corpus callosum of the human brain. *Coll Antropol* **30**(2), 375–381.

Jovanov-Milosevic N, Culjat M, Kostovic I (2009) Growth of the human corpus callosum: modular and laminar morphogenetic zones. *Front Neuroanat* **3**, 6.

Jovanov-Milosevic N, Petanjek Z, Petrovic D, et al. (2010) Morphology, molecular phenotypes and distribution of neurons in developing human corpus callosum. *Eur J Neurosci* **32**(9), 1423–1432.

Judas M, Milosevic NJ, Rasin MR, et al. (2003) Complex patterns and simple architects: molecular guidance cues for developing axonal pathways in the telencephalon. *Prog Mol Subcell Biol* **32**, 1–32.

Judas M, Rados M, Jovanov-Milosevic N, et al. (2005) Structural, immunocytochemical, and MR imaging properties of periventricular crossroads of growing cortical pathways in preterm infants. *AJNR Am J Neuroradiol* **26**(10), 2671–2684.

Judas M, Simic G, Petanjek Z, et al. (2011) The Zagreb Collection of human brains: a unique, versatile, but underexploited resource for the neuroscience community. *Ann N Y Acad Sci* **1225**(S1), 105–130.

Kania A, Klein R (2016) Mechanisms of ephrins signaling in morphogenesis, neural development and disase. *Nat Rev Mol Cell Biol* **17**(4), 240–256.

Kantor DB, Chivatakarn O, Peer KL, et al. (2004) Semaphorin 5A is a bifunctional axon guidance cue regulated by heparan and chondroitin sulfate proteoglycans. *Neuron* **44**(6), 961–975.

Karol EA, Pandya DN (1971) The distribution of the corpus callosum in the Rhesus monkey. *Brain* **94**(3), 471–486.

Kasprian G, Brugger PC, Weber M, et al. (2008) *In utero* tractography of fetal white matter development. *NeuroImage* **43**(2), 213–224.

Klein R (2004) Eph/ephrin signaling in morphogenesis, neural development and plasticity. *Curr Opin Cell Biol* **16** (5), 580–589.

Klein R, Kania A (2014) Ephrin signaling in the developing nervous system. *Curr Opin Neurobiol* **27**, 16–24.

Koester SE, O'Leary DD (1994) Axons of early generated neurons in cingulate cortex pioneer the corpus callosum. *J Neurosci* **14**(11), 6606–6620.

Kostovic I, Jovanov-Milosevic N (2006) The development of cerebral connections during the first 20-45 weeks' gestation. *Semin Fetal Neonatal Med* **11**(6), 415–422.

Kostovic I, Rasin MR, Petanjek Z, et al. (2002) Morphological characteristics of the cells in the subcallosal zone (nucleus septohippocampalis) of the human fetus. *Neuroembiology* **1**, 97–104.

Kostovic I, Jovanov-Milosevic N, Rados M, et al. (2014) Perinatal and early postnatal reorganization of the subplate and related cellular compartments in the human cerebral wall as revealed by histological and MRI approaches. *Brain Struct Funct* **219**(1), 231–253.

Lamantia AS, Rakic P (1990) Cytological and quantitative characteristics of four cerebral commissures in the rhesus monkey. *J Comp Neurol* **291**(4), 520–537.

LaMantia AS, Rakic P (1990) Axon overproduction and elimination in the corpus callosum of the developing rhesus monkey. *J Neurosci* **10**(7), 2156–2175.

Lent R, Uziel D, Baudrimont M, et al. (2005) Cellular and molecular tunnels surrounding the forebrain commissures of human fetuses. *J Comp Neurol* **483**(4), 375–382.

Leyva-Diaz E, Lopez-Bendito G (2013) In and out from the cortex: development of major forebrain connections. *Neuroscience* **254**, 26201.

Liewald D, Miller R, Logothetis N, et al. (2014) Distribution of axon diameters in cortical white matter: an electron-microscopic study on three human brains and a macaque. *Biol Cybern* **108**(5), 541–557.

Lindwall C, Fothergill T, Richards LJ (2007) Commissure formation in the mammalian forebrain. *Curr Opin Neurobiol* **17**, 3–14.

Lopez-Bendito G, Cautinat A, Sanchez JA, et al. (2006) Tangential neuronal migration controls axon guidance: a role for neuregulin-1 in thalamocortical axon navigation. *Cell* **125**, 127–142.

Luttenberg J (1966) Contribution to the fetal ontogenesis of the corpus callosum in man. 3. Myelinization in the corpus callosum. *Folia Morphol (Praha)* **14**(3), 192–199.

Matsunami K, Kawashima T, Ueki S, et al. (1994) Topography of commissural fibers in the corpus callosum of the cat: a study using WGA-HRP method. *Neurosci Res* **20**(2), 137–148.

Mendes SW, Henkemeyer M, Liebl DJ (2006) Multiple Eph receptors and B-class ephrins regulate midline crossing of corpus callosum fibers in the developing mouse forebrain. *J Neurosci* **26**(3), 882–892.

Miller SP, Ramaswamy V, Michelson D (2005) Patterns of brain injury in term neonatal encephalopathy. *J Pediatr* **146**(4), 453–460.

Niquille M, Garel S, Mann F, et al. (2009) Transient neuronal populations are required to guide callosal axons: a role for semaphorin 3C. *PLoS Biol* **7**(10), e1000230.

Nishikimi M, Oishi K, Nakajima K (2013) Axon guidance mechanisms for establishment of callosal connections. *Neural Plast* **2**, 149060.

Oh KJ, Kim SM, Hong JS, et al. (2017) Twenty-four percent of patients with clinical chorioamnionitis in preterm gestations have no evidence of either culture-proven intraamniotic infection or intraamniotic inflammation. *Am J Obstet Gynecol* **216** (6), 604.e1–604.e11.

Osen-Sand A, Catsicas M, Staple JK, et al. (1993) Inhibition of axonal growth by SNAP-25 antisense oligonucleotides *in vitro* and *in vivo*. *Nature* **364**(6436), 445–448.

Ozaki H, Wahlsten D (1992) Prenatal formation of the normal mouse corpus callosum: A quantitative study with carbocyanine dyes. *J Comp Neurol* **323**, 81–90.

Pandya DN, Karol EA, Heilbronn D (1971) The topographical distribution of interhemispheric projections in the corpus callosum of the rhesus monkey. *Brain Res* **32**(1), 31–43.

Paul LK (2011) Developmental malformation of the corpus callosum: a review of typical callosal development and examples of developmental disorders with callosal involvement. *J Neurodev Disord* **3**(1), 3–27.

Paul LK, Brown WS, Adolphs R, et al. (2007) Agenesis of the corpus callosum: genetic, developmental and functional aspects of connectivity. *Nat Rev Neurosci* **8**(4), 287–299.

Peters M, Jancke L, Zilles K (2000) Comparison of overall brain volume and midsagittal corpus callosum surface area as obtained from NMR scans and direct anatomical measures: a within-subject study on autopsy brains. *Neuropsychologia* **38** (10), 1375–1381.

Piper M, Plachez C, Zalucki O, et al. (2009) Neuropilin 1-sema signaling regulates crossing of cingulate pioneering axons during development of the corpus callosum. *Cereb Cortex* **19** (Suppl 1), 11–20.

Plachez C, Richards LJ (2005) Mechanisms of axon guidance in the developing nervous system. *Curr Top Dev Biol* **69**, 267–346.

Pont-Lezica L, Beumer W, Colasse S, et al. (2014) Microglia shape corpus callosum axon tract fasciculation: functional impact of prenatal inflammation. *Eur J Neurosci* **39**(10), 1551–1557.

Prins JR, Eskandar S, Eggen BJL, et al. (2018) Microglia, the missing link in maternal immune activation and fetal neurodevelopment; and a possible link in preeclampsia and disturbed neurodevelopment? *J Reprod Immunol* **126**, 18–22.

Rakic P, Yakovlev PI (1968) Development of the corpus callosum and cavum septi in man. *J Comp Neurol* **132**(1), 45–72.

Rash BG, Richards LJ (2001) A role for cingulate pioneering axons in the development of the corpus callosum. *J Comp Neurol* **434**(2), 147–157.

Ren T, Anderson A, Shen WB, et al. (2006) Imaging, anatomical, and molecular analysis of callosal formation in the developing

human fetal brain. *Anat Rec A Discov Mol Cell Evol Biol* **288** (2), 191–204.

Richards LJ, Plachez C, Ren T (2004) Mechanisms regulating the development of the corpus callosum and its agenesis in mouse and human. *Clin Genet* **66**(4), 276–289.

Rockland KS, Pandya DN (1986) Topography of occipital lobe commissural connections in the rhesus monkey. *Brain Res* **365** (1), 174–178.

Romero R, Chaemsaithong P, Korzeniewski SJ, et al. (2016) Clinical chorioamnionitis at term II: the intra-amniotic inflammatory response. *J Perinat Med* **44**(1), 5–22.

Sato Y, Hirata T, Ogawa M, et al. (1998) Requirement for early generated neurons recognized by monoclonal antibody lot1 in the formation of lateral olfactory tract. *J Neurosci* **18**, 7800–7810.

Schmahmann J, Pandya D (2006) *Fiber pathways of the brain*, pp. 485–496. New York: Oxford University Press.

Schwartz ML, Goldman-Rakic PS (1991) Prenatal specification of callosal connections in rhesus monkey. *J Comp Neurol* **307**, 144–162.

Schwartz ML, Rakic P, Goldman-Rakic PS (1991) Early phenotype expression of cortical neurons: evidence that a subclass of migrating neurons have callosal axons. *Proc Natl Acad Sci U S A* **88**, 1354–1358.

Seltzer B, Pandya DN (1983) The distribution of posterior parietal fibers in the corpus callosum of the rhesus monkey. *Exp Brain Res* **49**(1), 147–150.

Shu T, Li Y, Keller A, et al. (2003) The glial sling is a migratory population of developing neurons. *Development* **130**, 2929–2937.

Silver BJ, Lorenz SE, Wahlsten D, et al. (1982) Axonal guidance during development of the great cerebral commissures: descriptive and experimental studies, *in vivo*, on the role of preformed glial pathways. *J Comp Neurol* **210**, 10–29.

Sretavan DW, Pure E, Siegel MW, et al. (1995) Disruption of retinal axon ingrowth by ablation of embryonic mouse optic chiasm neurons. *Science* **269**, 98–101.

Suarez R, Gobius I, Rischards LJ (2014) Evolution and development of interhemispheric connections in the vertebrate forebrain. *Front Hum Neurosci* **8**, 497.

Tovar-Moll F, Moll J, de Oliveira-Souza R, et al. (2007) Neuroplasticity in human callosal dysgenesis: a diffusion tensor imaging study. *Cereb Cortex* **17**(3), 531–541.

Valentino KL, Jones EG (1982) The early formation of the corpus callosum: a light and electron microscopic study in foetal and neonatal rats. *J Neurocytol* **11**(4), 583–609.

Van den Heuvel DMA, Hellemons AJCGM, Pasterkamp RJ (2013) Spatiotemporal expression of repulsive guidance molecules (RGMs) and their receptor neogenin in the mouse brain. *PLoS ONE* **8**(2), e55828.

Verney C, Monier A, Fallet-Bianco C, et al. (2010) Early microglial colonization of the human forebrain and possible involvement in periventricular white-matter injury of preterm infants. *J Anat* **217**(4), 436–448.

Wahl M, Lauterbach-Soon B, Hattingen E, et al. (2007) Human motor corpus callosum: topography, somatotopy, and link between microstructure and function. *Neuroscience* **27**, 12132–12138.

Wahl M, Strominger Z, Jeremy RJ, et al. (2009) Variability of homotopic and heterotopic callosal connectivity in partial agenesis of the corpus callosum: a 3T diffusion tensor imaging and Q-ball tractography study. *AJNR Am J Neuroradiol* **30**, 282–2.

Wiggins CJ, Schäfer A, Dhital B, et al. (2007) After over 200 years, 7 T magnetic resonance imaging reveals the foliate structure of the human corpus callosum *in vivo*. *Br J Radol* **90** (1073), 20160906.

Wilson NH, Key B (2006) Neogenin interacts with RGMa and Netrin-1 to guide axons within the embryonic vertebrate forebrain. *Dev Biol* **296**(2), 485–498.

Witelson SF (1989) Hand and sex differences in the isthmus and genu of the human corpus callosum. A postmortem morphological study. *Brain* **112**(Pt 3), 799–835.

Wu PM, Shih HI, Yu WH, et al. (2018) Corpus callosum and cerebellar vermis size in very preterm infants: Relationship to long-term neurodevelopmental outcome. *Pediatr Neonatol* **S1875–9572**(17), 30546–6.

Yang Z, Suzuki R, Daniels SB, et al. (2006) NG2 glial cells provide a favourable substrate for growing axons. *J Neurosci* **26** (14), 3829–3839.

Yang M, Wu M, Xia P, et al. (2012) The role of microtubule-associated protein 1B in axonal growth and neuronal migration in the central nervous system. *Neural Regen Res* **7**(11), 842gen R.

Zanin E, Ranjeva JP, Confort-Gouny S, et al. (2011) White matter maturation of normal human fetal brain. An *in vivo* diffusion tensor tractography study. *Brain Behav* **1**(2), 95–108.

Zhou J, Wen Y, She L, et al. (2013) Axon position within the corpus callosum determines contralateral cortical projection. *Proc Natl Acad Sci U S A* **110**(29), E2714–E2723.